### Soft Matter



PAPER View Article Online
View Journal | View Issue



**Cite this:** *Soft Matter*, 2023, **19**. 7717

Received 23rd July 2023, Accepted 6th September 2023

DOI: 10.1039/d3sm00961k

rsc.li/soft-matter-journal

# Structural color from pigment-loaded nanostructures†

Tianqi Sai,<sup>a</sup> Luis S. Froufe-Pérez,<sup>b</sup> Frank Scheffold,<sup>b</sup> Bodo D. Wilts on and Eric R. Dufresne \*\*D\*\*ad

Color can originate from wavelength-dependence in the absorption of pigments or the scattering of nanostructures. While synthetic colors are dominated by the former, vivid structural colors found in nature have inspired much research on the latter. However, many of the most vibrant colors in nature involve the interactions of structure and pigment. Here, we demonstrate that pigment can be exploited to efficiently create bright structural color at wavelengths outside its absorption band. We created pigment-enhanced Bragg reflectors by sequentially spin-coating layers of poly-vinyl alcohol (PVA) and polystyrene (PS) loaded with  $\beta$ -carotene (BC). With only 10 double layers, we achieved a peak reflectance over 0.8 at 550 nm and normal incidence. A pigment-free multilayer made of the same materials would require 25 double layers to achieve the same reflectance. Further, pigment loading suppressed the Bragg reflector's characteristic iridescence. Using numerical simulations, we further show that similar pigment loadings could significantly expand the gamut of non-iridescent colors addressable by photonic glasses.

#### I. Introduction

Structural colors arise from the interference of light scattered from nanostructures.<sup>1</sup> Nanostructures with long-range order, such as photonic crystals, can produce bright saturated colors across the full visible spectrum. However, these colors tend to vary strongly with viewing angle, *i.e.* they are iridescent.<sup>2,3</sup> Nanostructures with only short-range order, such as photonic glasses, produce non-iridescent colors. However, they tend to be less bright and less saturated, particularly at longer wavelengths.<sup>4–7</sup> In this case, color saturation can be improved by suppressing multiple scattering through the incorporation of low-concentrations of a broad-band absorber.<sup>8</sup>

Ideally, one could combine the advantages of these two approaches, and generate structural colors with both low-angle dependence and high saturation. Structure-pigment interactions can play a key role in achieving this goal. Natures most vibrant colors often result from a finely tuned interplay between structural and pigmentary color. 9,10 Some evidence in

In day-to-day life, we create vivid non-iridescent color by starting with a white base and adding pigment. The white base scatters strongly across wavelengths, and diffusely reflects most of the light incident upon it. High-index nanoparticles, such as titanium dioxide or polysytrene, are typically employed as a scattering base. Scattering is characterised by the transport mean-free path,  $\ell_{\rm mfp}$ , which describes how far light propagates through a material before forgetting its original propagation direction. Pigment absorbs light over a range of wavelengths. The absorption length,  $\ell_{\rm abs}$ , characterizes how far a typical photon travels into a material before it is absorbed. Wavelengths where  $\ell_{\rm mfp} \gg \ell_{\rm abs}$  are absorbed within the material. Wavelengths where  $\ell_{\rm abs} \gg \ell_{\rm mfp}$  are diffusely reflected at high efficiency.

The contributions of scattering and absorption, however, are not always easy to separate. They are intimately related, because they both derive from the same material property: the dielectric function. The real part of the dielectric function determines the refractive index, which leads to scattering. The imaginary part of the dielectric function determines absorption. The real and imaginary parts of the dielectric function cannot be varied independently but must satisfy the Kramers–Kronig relation. As a consequence, broad-band absorbers, like melanin, can feature an elevated index of refraction ( $n \sim 1.7$ ) across the visible range. Melanin nanostructures are widely used in nature for the creation of vivid colors. Fecently, researchers

biological systems suggests that the combined mechanisms can create colors and optical properties unachievable by either mechanism alone. 11,12

<sup>&</sup>lt;sup>a</sup> Department of Materials, ETH Zürich, 8093 Zürich, Switzerland. E-mail: eric.r.dufresne@cornell.edu

<sup>&</sup>lt;sup>b</sup> Department of Physics, University of Fribourg, 1700 Fribourg, Switzerland

<sup>&</sup>lt;sup>c</sup> Department of Chemistry and Physics of Materials University of Salzburg, 5020 Salzburg, Austria

<sup>&</sup>lt;sup>d</sup> Department of Materials Science and Engineering, Department of Physics, Cornell University, Ithaca, NY, 14850, USA

<sup>†</sup> Electronic supplementary information (ESI) available. See DOI: https://doi.org/10.1039/d3sm00961k

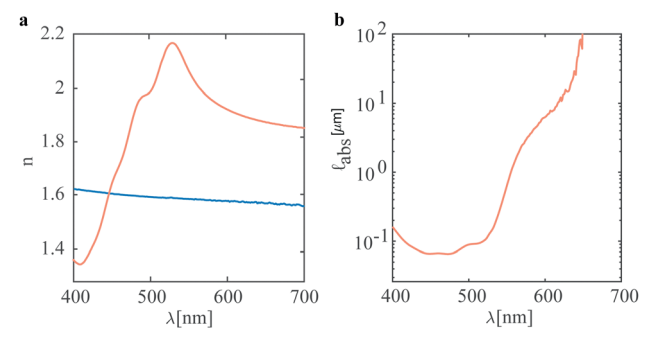


Fig. 1 Effect on beta-carotene (BC) loading on the optical properties of polystyrene (PS). (a) Measured refractive index, n, of pure PS (blue) and 40% BC/PS (orange) (b) measured absorption length,  $\ell_{abs}$ ) of 40% BC/PS.

have employed synthetic melanin to produce structural colors. 16-19

Absorbing materials can achieve even higher indices of refraction, but are challenging to use for structural coloration. Broadband absorbers with higher refractive indices are inappropriate for structural color applications because  $\ell_{abs}$  becomes too small to enable constructive interference. Consider familiar amorphous carbon. It absorbs strongly across the visible spectrum and features refractive indices approaching 2.5.20 However, its absorption length is much shorter than the wavelength of light, making

constructive interference impossible. Semiconductors are a more suitable choice. Titanium dioxide has low absorption across the visible spectrum, but absorbs strongly at shorter wavelengths. Thanks to the Kramers-Kronig relation, it features a refractive index exceeding 2.5 across the visible spectrum. 21 From an optics perspective, this is a perfect candidate for structural color. From a materials perspective, however, there are no scalable methods currently available for creating photonic nanostructures from this material. Nevertheless, titanium dioxide remains a excellent example of how absorption over one range of wavelengths can increase the refractive index at wavelengths outside the absorption band.

To fuse processibility and high refractive index, absorbing polymers are a promising choice. UV-absorbing pigments are frequently added to increase the refractive index in the visible spectrum, and provide a modest increase of the refractive index  $(\Delta n \approx 0.07)^{22-24}$  Recently, very high refractive indices in the visible were achieved by blending an everyday polymer, polystrene, with a common plant-based pigment, beta-carotene.<sup>25</sup> In that case, refractive indices as high as 2.2 were achieved near the absorption edge (about 525 nm) and decayed slowly to 1.75 at 700 nm.

In this work, we demonstrate how pigment-enhanced scattering in a processable polymer can be exploited to achieve high-reflectance structural colors. Through a combination of

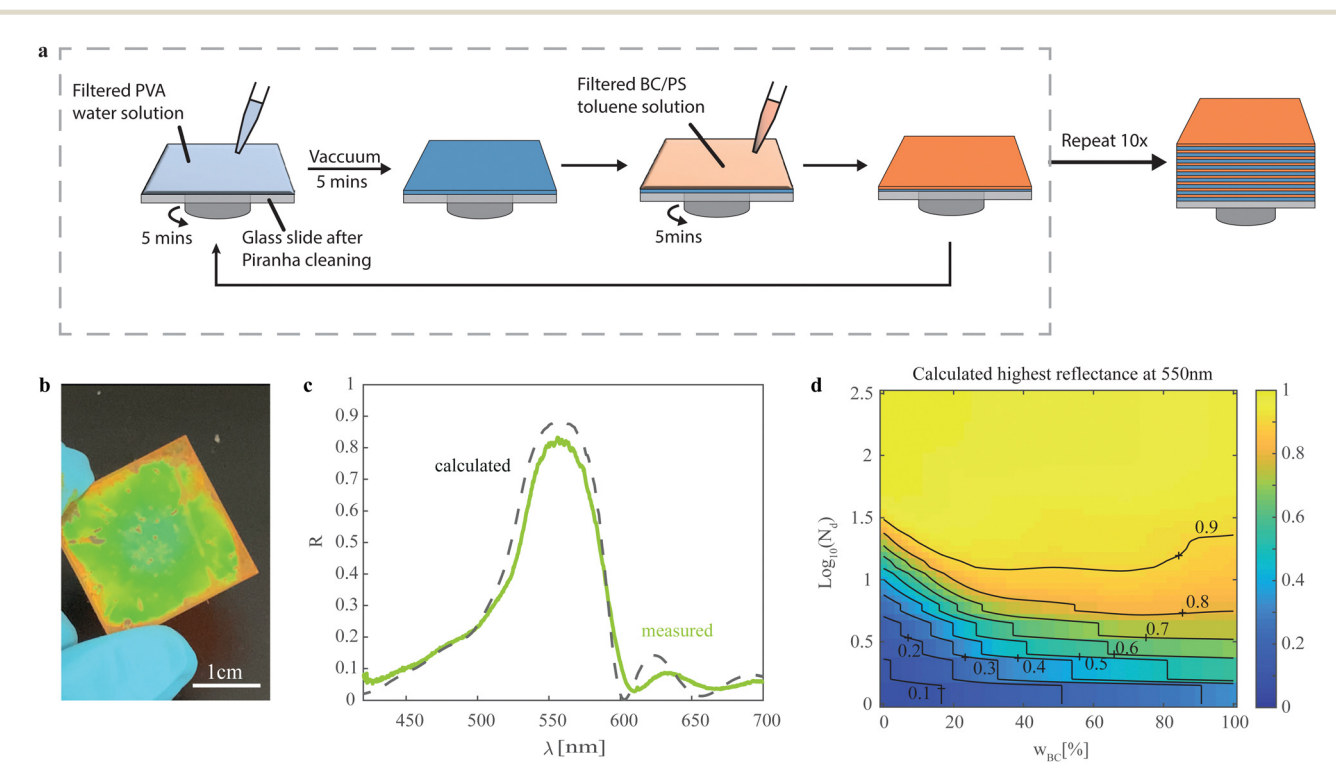


Fig. 2 Enhanced reflectance of pigment-loaded multilayered reflectors. (a) Schematic diagram of the preparation procedure of a 10-double layer reflector made of alternating 40%BC/PS and PVA films. (b) Photo of the prepared reflector. (c) Reflectance of a 10-double layer Bragg reflector, consisting of alternating 40%BC/PS and PVA films, at normal incidence. Each 40%BC/PS layer is 57 nm thick and each PVA layer is 112 nm thick. The substrate is a plain glass slide. Average measured result of three different point is shown as a green solid line. The prediction from T-matrix calculations is shown as a dark gray dashed line. (d) Colormap of calculated peak reflectance at the wavelength of 550 nm for multilayers with different number of repeating doublelayers,  $N_d$ , and different BC concentrations in PS,  $w_{BC}$ . The optical properties at arbitary concentrations were determined by linear interpolation of the ellipsometry data in ref. 25

experiment and simulation, we demonstrate how engineered absorption can simplify the production of Bragg mirrors and remove iridescence while maintaining brightness and saturation. Using numerical simulation, we show that the interplay of absorption and scattering can expand the gamut of photonic glasses.

#### II. Results and discussion

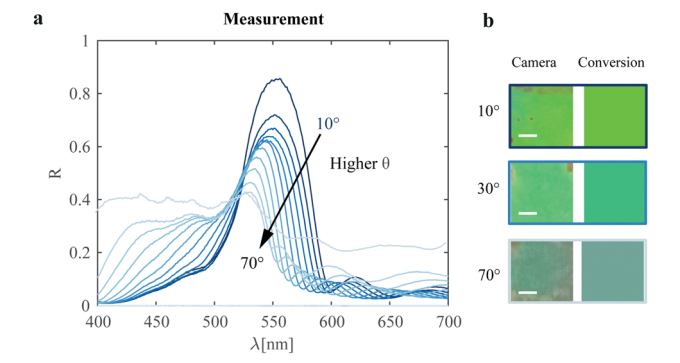
#### A. Optical properties of BC/PS blends

Following, 25 we prepared thin composite films of polystyrene (PS) loaded with beta-carotene (BC). Their optical properties were characterized by ellipsometry. Results for a PS film loaded with 40% BC, by weight, are shown in Fig. 1. The blend absorbs strongly at wavelengths up to about 525 nm. The refractive index peaks to 2.15 at 528 nm, and decays slowly to 1.8 at 700 nm. Unfortunately, the absorption length is only 150 nm at the peak refractive index. This precludes use for structurally colored materials, where light needs to constructively interfere across multiple reflections. However, with a small shift of wavelength off the peak (to 550 nm), the refractive index enhancement remains highly elevated (n = 2.03), but the absorption length increases by a factor of 7 to 1.12  $\mu$ m. While this is too short for applications involving bulk propagation, we will show that it can be effectively exploited for nanophotonic applications.

#### B. Design and fabrication of a pigment-enhanced Bragg reflector

To demonstrate the feasibility of pigment-loaded polymers for structural color, we created Bragg reflectors based on BC-loaded PS blends. Bragg reflectors are periodic stacks of alternating dielectric layers whose spacing is optimized to constructively reinforce reflected light over a specific range of wavelengths. We fabricated Bragg reflectors using a sequential spin coating method, 26,27 shown schematically in Fig. 2. In this approach, the solvents of the alternating polymers must be mutually orthogonal. At the same time, each solution should have reasonable wettablity on films of the previous polymer. Commonly, UV ozone or plasma treatment is used between the spinning of each layer to increase the wettablity and to allow the successful deposition of the next layer.<sup>28,29</sup> However, BC is degraded by these treatments. After exploring a wide range of solvent and polymer combinations, we settled on BC/PS in toluene and polyvinyl alcohol (PVA, n = 1.48 at 550 nm) in water.<sup>27</sup>

The thicknesses of the polymer layers were optimized using transfer matrix simulations, 30 implemented in MATLAB. 31 To find the optimal layer thicknesses, we fixed the materials to PVA and 40% BC/PS, and the number of double-layers to 10. We varied the thickness of each double layer, d, from 120 nm to 250 nm and the thickness of the high index layer,  $t_h$  from 0 to d. We determined the thickness combination which gave the highest reflectance for each wavelength from 400 to 700 nm. Outside the absorption band, the optimal thickness followed the classic quarter-wave design rule, 30,32 as shown in Fig. S1(a)-(c) (ESI†). The highest reflectivity, about 80%, was found at



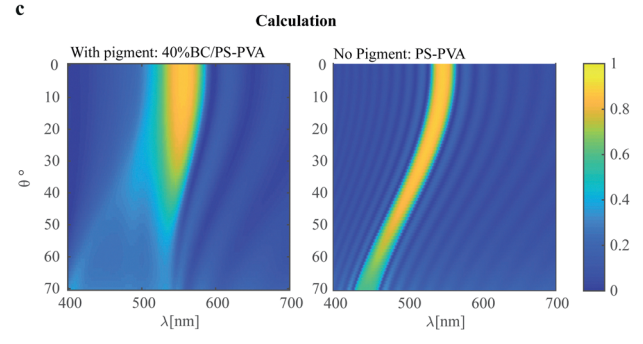


Fig. 3 Reduced iridescence of pigment-loaded Bragg reflector. (a) Measured specular reflectance at different angles of incidence, from  $10^{\circ}$  to  $70^{\circ}$ with an interval of 5°, of a 10-doublelayer Bragg reflector, consisting of alternating 40%BC/PS (57 nm) and PVA (112 nm) films. (b) Photos of the Bragg reflector taken at different angles, and the corresponding RGB color swatches determined from the reflectance spectrum. Scale bar: 1 mm. (c) T-matrix predication of the specular reflectance spectra at different angles of incidence. On the left, results for a 10-doublelayer Bragg reflector, consisting of alternating 40%BC/PS (57 nm) and PVA (112 nm) films. On the right, results for a 25-double layer Bragg reflector, consisting of alternating PS (87 nm) and PVA (90 nm) films. The thicknesses combinations are chosen to give the highest reflectance at the wavelength of 550 nm.

550 nm, near the edge of the absorption band (Fig. S1d, ESI†) There, 40% BC/PS features a refractive index of n = 2.03 and absorption length of  $\ell_{abs}$  = 1.12  $\mu m$ .

#### C. Characterization and analysis of a pigment-enhanced **Bragg reflector**

To realize this design, we fabricated a 10 double-layer reflector made of alternating 57 nm thick 40% BC/PS and 112 nm thick PVA films. The cm-scale film had a vivid green appearance, as shown in Fig. 2b. Specular reflectance gave the film a mirrorlike appearance, shown in the Movie S1 (ESI†). We measured the spectrum of reflected light at normal incidence, shown as a solid line in Fig. 2c. The spectrum had a peak reflectance of 83% in a band near 550 nm, and showed excellent agreement with the spectrum predicted from T-matrix calculations (dashed line in Fig. 2c).

To explore the benefits and limitations of pigmentenhanced Bragg mirrors, we used the T-matrix approach to calculate the reflectance for a range of Bragg reflectors. Fig. 2d shows the peak reflectance at 550 nm for BC loadings,  $w_{\rm BC}$ , from 0 to 100%, and numbers of double layers,  $N_d$ , from 1 to 316. Black lines show contours of constant reflectance. At low Paper Soft Matter

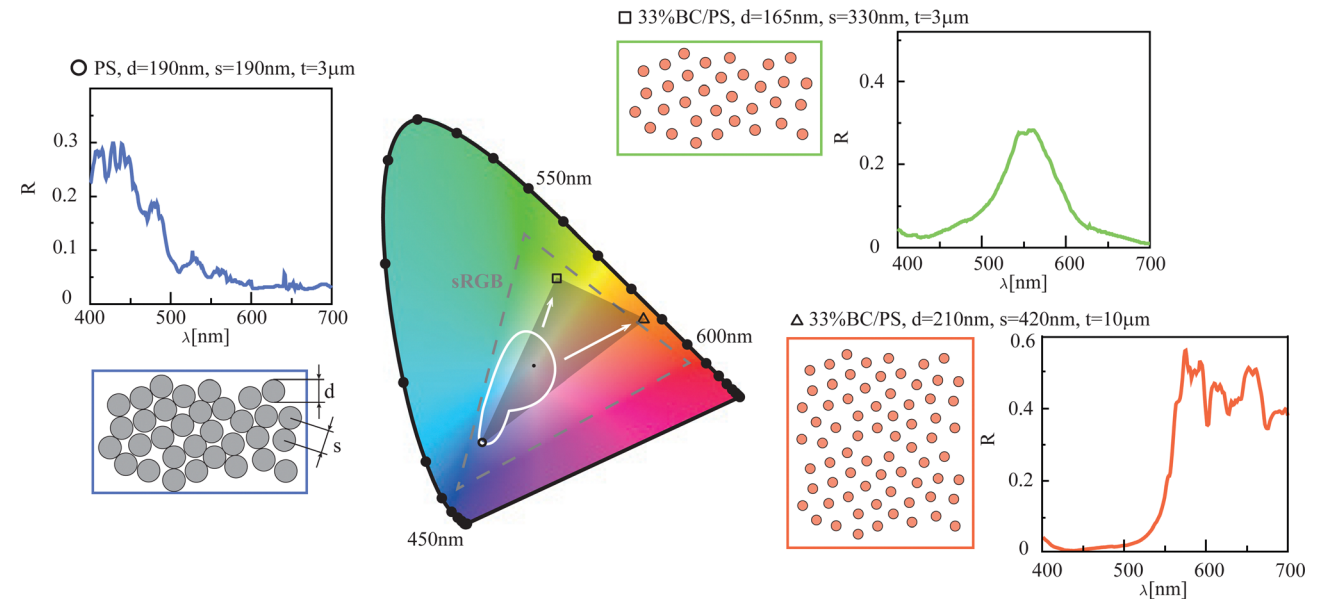


Fig. 4 Extending the gamut of photonic glasses with the help of pigments. In the center is the CIE chromaticity diagram, with the sRGB gamut indicated by a gray dashed line. The white line outlines the simulated gamut achieved by amorphous assemblies of pigment-free polystyrene particles. The most saturated blue is marked as a white circle. With the help of BC, simulations of photonic glasses with varying size, spacking and thickness revealed relatively saturated green (square) and orange-red (triangle) hues. The geometries and spectra of the corresponding photonic glasses are shown in neighboring plots. Note that particle centers are always generated from jammed sphere packings, even when d < s in the optical simulations. Green (square):33% BC/PS composite particle assembly with a film thickness of 3  $\mu$ m, a particle diameter of 165 nm and a particle spacing of 330 nm (square). Red (triangle): 98 particle assembly with a film thickness of 3  $\mu$ m, a particle diameter of 210 nm and a particle spacing of 420 nm. Blue (circle): PS particle assembly with a film thickness of 3  $\mu$ m, a particle diameter of 190 nm and a particle spacing of 190 nm.

pigment concentrations,  $N_{\rm d}$  decreases exponentially with  $w_{\rm BC}$ . However, the effect of added pigment saturates, particularly for high reflectance. For a target reflectance of 90%, the required number of double layers,  $N_{\rm d}$ , drops from 32 to 13 double layers as the BC loading reaches 27%. Additional BC offers no further improvement. At 80% reflectivity,  $N_{\rm d}$  is reduced by more than a factor of three, from 25 to 8 double layers, at  $w_{\rm BC}$  = 40%. Again, additional pigment loading offers little benefit. The benefit of pigment-loading is strongest as the refractive-index difference between the undoped layers vanishes (Fig. S2, ESI†) and for wavelengths at the edge of the absorption band (Fig. S3, ESI†).

Pigment-loaded Bragg reflectors not only require fewer double layers, but also show reduced iridescence. The specular reflectance of the film measured at different incident angles is shown in Fig. 3a. With higher angles of incidence, the reflectance peak vanished, while shifting slightly from 550 nm to 525 nm. Images of the film viewed in specular reflection are shown in Fig. 3b. At low angles (close to normal incidence), the film shows bright and saturated greens. At higher angles, the color is dulled. There is good agreement between the measured reflectance spectra and the observed color. To the right of each photo, we show the RGB color inferred from the measured reflectance spectrum using the open source python package colorpy. These results are in good agreement with T-matrix simulations, shown on the left of Fig. 3c. For comparison, the calculated reflectance spectra from a conventional Bragg mirror (PS-PVA without pigment) are shown in the right panel of Fig. 3c. This pigment-free reference was designed to give the same peak reflectance at the wavelength of 550 nm and normal incidence. In the pigment-free case, we observe a strong shift to shorter wavelengths in the reflectance at larger angles of incidence. This iridescence is a characteristic feature of conventional Bragg reflectors. In the pigment loaded mirror, iridescence is suppressed because the peak wavelength is shifted into the absorption band of the pigment.

## D. Pigment-enhanced scattering could extend the gamut of photonic glasses

Having established the viability of pigment-enhanced structural color in Bragg mirrors, we used finite-difference-time-domain simulations to explore its potential in photonic glasses. Photonic glasses are excellent contrasts to Bragg mirrors. While the former are 3-D and feature only short-range correlations, the latter are 1-D and have perfect long-range order. Photonic glasses are made from jammed packings of hard spheres using the protocol described in ref. 33.

Our explorations suggest that pigment-loading could significantly expand the palette of photonic glasses. Without absorption, the gamut from plain polystyrene assemblies is outlined on the CIE colorspace with a white line in Fig. 4. The results of individual simulations, with varying particle size and spacing, are shown in Fig. S4 (ESI†). This gamut is largely limited to the unsaturated center of the diagram, but accesses some relatively saturated blues. With a loading of 33% BC inside the PS particles, the gamut can be remarkably extended, as indicated by the gray triangle in the CIE diagram of Fig. 4. The most

highly saturated red, green, and blue we were able to create are found at the corners of the triangle. This extended gamut fills a large fraction of with the sRGB gamut (shown as a grey dashed triangle), the standard color space for the internet.<sup>34</sup>

The function of the pigment is markedly different in the saturated green and red samples. For the green sample, the color emerges thanks to the enhanced refractive index of the BC/PS blend in the green. This leads to enhanced scattering and structural color. For the red sample, the color emerges from broadband scattering and the absorption of BC/PS at short wavelengths, similar to a conventional paint. While the first mechanism is sensitive to the thickness of the sample, the second is not, see Fig. S4 (ESI†).

#### III. Conclusion and outlook

Our results show that the pigment can enhance the efficiency and gamut of structurally-colored materials. For Bragg reflectors, pigment can create high-brightness colors with reduced angledependence and less material. For photonic glasses, the same pigment can be used to create one color through pigmentenhanced scattering, or another though conventional absorption in a broad-band scattering medium.

While the assembly of a pigment-loaded Bragg mirror via sequential spin-coating was sufficient for proof-of-principle, the integration of pigments into self-assembled Bragg mirrors<sup>35</sup> would simplify processing. Several challenges in materials chemistry and processing must be overcome to realize the photonic glasses proposed in this work. For example, new synthetic approaches are required to produce monodisperse polymer nanoparticles with high pigment loadings. In the meantime, a systematic numerical exploration of the design space would more clearly define the benefits and limitations of this approach.

#### IV. Materials and methods

#### A. Materials

BC (synthetic,  $\geq$  93% (UV)), PS (35 kDa (used for making films and multilayers) and 192 kDa (used for processability experiments)), PVA ( $M_{\rm w}$  85 000–124 000, 99+% hydrolyzed), toluene and dichloromethane were bought from Sigma-Aldrich and used as received.

#### B. Spin coating

For the preparation of the PVA aqueous solution(2%), 2 g PVA powder was added into 100 mL of Milli-Q water. Once added, the solution was stirred vigorously on a hotplate at 95 for one hour to obtain a homogenous solution. For the preparation of the 40% BC/PS toluene solution (10 mg per mL), 60 mg BC, 90 mg PS and 15 mL toluene were added to a 15 mL glass vial (to minimize the amount of air left in the vial). Then, the vial was sealed, and the solution was stirred at 800 rpm for 30 minutes. The glass vial was covered with aluminum foil during stirring to avoid light. After stirring, the solution was filtered using a syringe filter (pore size 0.45 µm).

The glass slide (2.5 cm  $\times$  2.5 cm) for spin coating was used after piranha cleaning. For the deposition of multilayers, 1 mL PVA solution was first spread on the glass slide and spun at 1500 rpm for 5 min. After spinning, the film was vacuumed in a vacuum chamber for at least 5 minutes to dry out the water completely before the deposition of the next BC/PS layer. To deposit the BC/PS layer, 0.5 mL BC/PS toluene solution was spread on the dried PVA layer and spun at 2000 rpm for 5 min. The same procedure was repeated 10 times for the preparation of every double layer, as shown in Fig. 2a. The spectrum of the prepared film was characterized freshly right after preparation.

#### C. Ellipsometry

A spectroscopic ellipsometer (M2000, J. A. Woollam) was used to measure the phase and amplitude change of light after interacting with the samples. All measurements were performed between 250 and 1000 nm at an angle of incidence 65°, and all data were acquired and analyzed using WVASE software. Since the films are transparent at longer wavelengths, the films were regarded as a homogeneous material with the thickness fitted by Cauchy dispersion relation in the wavelength range from 600 to 1000 nm, After the film thickness was determined and fixed, the optical constants, refractive indices n and extinction coefficient  $\kappa$  were fitted using point to point fitting mode.

#### D. Reflectance measurement

The reflectance at normal incidence of the prepared Bragg reflector was measured on a microscope (Nikon Ti2) with a  $60 \times$  air objective (S Plan Fluor ELWD, NA = 0.7). The light source is a broadband halogen fiber-coupled illuminator (Thorlabs OSL2). The field aperture and the angular aperture on the microscope were closed to the minimum to reduce the spot size and cut off higher angle reflectance. The final spot size was around 50 μm, and the collecting angle was about 15°. The reflected light was collected by a light detector (Ocean Optics, Ocean HDX). The reflectance was measured at three different points and averaged.

The specular reflectance of the films have been measured with an angle-resolved spectrophotometry setup. The light source is a deuterium-halogen lamp (Ocean Optics DH-2000-BAL), ranging from 200 nm to 1000 nm. The sample is placed on a rotating stage and can be tilted to the desired angles. Finally, a light detector (Ocean Optics, QE Pro) is mounted on a rotating arm, which is controlled by software. The incident angle varied from  $10^{\circ}$  to  $70^{\circ}$ .

For both setups absolute reflectance is calculated using reflection from a broadband dielectric mirror Thorlabs, BBSQ2-E02) at the same incident angle. During the reflectance measurements, a layer of translucent Scotch tape was applied on the back side of the glass substrate to suppress unwanted back reflection from the glass-air interface.

#### E. FDTD simulations

In this work, the optical properties of 3D photonic glasses of strongly correlated hard spheres were calculated. Maximally random jammed assemblies were generated using the algorithm

presented in ref. 33. A collection of Poisson-distributed points is taken as an initial configuration in a periodic box. Points are grown in diameter at a certain rate, while collisions are taken into account to avoid overlap until the desired packing fraction is reached. The samples were generated using the C++ sphere packing code available in https://torquato.princeton.edu/linksand-codes/(available upon registration). In the examples shown, a packing fraction of 64.5% is reached. Each simulation considers the optical responses of 1000-3000 of spheres.

The optical properties of the generated structures were then calculated using LUMERICAL, a commercial-grade software using the FDTD method. Periodic boundary conditions in the lateral Y and Z direction, which are perpendicular to the incoming beam, and perfect matching layer boundaries in the X direction were used in all of the calculations. The incoming source was set as a plane wave.

#### Conflicts of interest

There are no conflicts to declare.

#### Acknowledgements

We acknowledge the Swiss National Science Foundation, National Centre of Competence in Research 'Bio-Inspired Materials' for funding, as well as Miguel Castillo and Ullrich Steiner for helpful discussions.

#### References

- 1 M. Kolle and S. Lee, Progress and Opportunities in Soft Photonics and Biologically Inspired Optics, Adv. Mater., 2018, 30(2), 1702669.
- 2 A. E. Seago, P. Brady, J. P. Vigneron and T. D. Schultz, Gold Bugs and beyond: A Review of Iridescence and Structural Colour Mechanisms in Beetles (Coleoptera), J. R. Soc., Interface, 2009, 6(suppl 2), S165-S184.
- 3 S. Kinoshita and S. Yoshioka, Structural Colors in Nature: The Role of Regularity and Irregularity in the Structure, Chem. Phys. Chem., 2005, 6(8), 1442-1459.
- 4 S. Magkiriadou, J. G. Park, Y. S. Kim and V. N. Manoharan, Absence of Red Structural Color in Photonic Glasses, Bird Feathers, and Certain Beetles, Phys. Rev. E, 2014, 90(6), 062302.
- 5 A. Kawamura, M. Kohri, G. Morimoto, Y. Nannichi, T. Taniguchi and K. Kishikawa, Full-Color Biomimetic Photonic Materials with Iridescent and Non-Iridescent Structural Colors, Sci. Rep., 2016, 6, 33984.
- 6 L. Schertel, L. Siedentop, J. M. Meijer, P. Keim, C. M. Aegerter and G. J. Aubry, et al., The Structural Colors of Photonic Glasses, Adv. Opt. Mater., 2019, 7(15), 1900442.
- 7 G. Jacucci, S. Vignolini and L. Schertel, The Limitations of Extending Nature's Color Palette in Correlated, Disordered Systems, Proc. Natl. Acad. Sci. U. S. A., 2020, 117(38), 23345-23349.

- 8 J. D. Forster, H. Noh, S. F. Liew, V. Saranathan, C. F. Schreck and L. Yang, et al., Biomimetic Isotropic Nanostructures for Structural Coloration, Adv. Mater., 2010, 22(26-27), 2939-2944.
- 9 D. G. Stavenga, Thin Film and Multilayer Optics Cause Structural Colors of Many Insects and Birds, Mater. Today: Proc., 2014, 1, 109-121.
- 10 M. J. Henze, O. Lind, B. D. Wilts and A. Kelber, Pterinpigmented nanospheres create the colours of the polymorphic damselfly Ischnura elegans, J. R. Soc., Interface, 2019, 16(153), 20180785.
- 11 B. D. Wilts, B. Wijnen, H. L. Leertouwer, U. Steiner and D. G. Stavenga, Extreme refractive index wing scale beads containing dense pterin pigments cause the bright colors of pierid butterflies, Adv. Opt. Mater., 2017, 5(3), 1600879.
- 12 K. Shavit, A. Wagner, L. Schertel, V. Farstey, D. Akkaynak and G. Zhang, et al., A tunable reflector enabling crustaceans to see but not be seen, Science, 2023, 379(6633), 695-700.
- 13 V. Lucarini, Kramers-Kronig Relations in Optical Materials Research, Springer, Berlin, 2005.
- 14 B. D. Wilts, K. Michielsen, H. D. Raedt and D. G. Stavenga, Sparkling Feather Reflections of a Bird-of-Paradise Explained by Finite-Difference Time-Domain Modeling, Proc. Natl. Acad. Sci. U. S. A., 2014, 111(12), 4363-4368.
- 15 J. Sun, B. Bhushan and J. Tong, Structural coloration in nature, RSC Adv., 2013, 3(35), 14862-14889.
- 16 M. Xiao, Y. Li, M. C. Allen, D. D. Deheyn, X. Yue and J. Zhao, et al., Bio-Inspired Structural Colors Produced via Self-Assembly of Synthetic Melanin Nanoparticles, ACS Nano, 2015, 9(5), 5454-5460.
- 17 M. Xiao, Z. Hu, Z. Wang, Y. Li, A. D. Tormo and N. Le Thomas, et al., Bioinspired Bright Noniridescent Photonic Melanin Supraballs, Sci. Adv., 2017, 3(9), e1701151.
- 18 S. Cho, T. S. Shim, J. H. Kim, D. H. Kim and S. H. Kim, Selective Coloration of Melanin Nanospheres through Resonant Mie Scattering, Adv. Mater., 2017, 29(22), 1700256.
- 19 C. M. Heil, A. Patil, B. Vanthournout, S. Singla, M. Bleuel and J. J. Song, et al., Mechanism of structural colors in binary mixtures of nanoparticle-based supraballs, Sci. Adv., 2023, **9**(21), eadf2859.
- 20 E. Arakawa, M. Williams and T. Inagaki, Optical properties of arc-evaporated carbon films between 0.6 and 3.8 eV, J. Appl. Phys., 1977, 48(7), 3176-3177.
- 21 J. R. DeVore, Refractive indices of rutile and sphalerite, JOSA., 1951, 41(6), 416-419.
- 22 T. Hanemann and K. Honnef, Tailoring the optical and thermomechanical properties of polymer host-guest systems, J. Appl. Polym. Sci., 2011, 122(6), 3514-3519.
- 23 T. Hanemann and K. Honnef, Viscosity and refractive index tailored methacrylate-based polymers, J. Appl. Polym. Sci., 2014, 131, 9.
- 24 T. Magrini, F. Bouville, A. Lauria, H. Le Ferrand, T. P. Niebel and A. R. Studart, Transparent and tough bulk composites inspired by nacre, *Nat. Commun.*, 2019, **10**(1), 2794.
- 25 M. Yasir, T. Sai, A. Sicher, F. Scheffold, U. Steiner and B. D. Wilts, et al., Enhancing the Refractive Index of Polymers with a Plant-Based Pigment, Small, 2021, 17(44), 2103061.

- 26 M. Kolle, Photonic structures inspired by nature, Springer Science & Business Media, 2011.
- 27 M. A. Castillo, C. Estévez-Varela, W. P. Wardley, R. Serna, I. Pastoriza-Santos and S. Núñez-Sánchez, et al., Enhanced light absorption in all-polymer biomimetic photonic structures by near-zero-index organic matter, Adv. Funct. Mater., 2022, 32(21), 2113039.
- 28 J. Wei, Z. Fang, J. Peng, W. Cai, Z. Zhu and R. Yao, et al., High-Performance Spin-Coated Aluminum Oxide Dielectric Fabricated by a Simple Oxygen Plasma-Treatment Process, J. Phys. D: Appl. Phys., 2018, 51(36), 365101.
- 29 J. Kasanen, M. Suvanto and T. T. Pakkanen, Self-Cleaning, Titanium Dioxide Based, Multilayer Coating Fabricated on Polymer and Glass Surfaces, J. Appl. Polym. Sci., 2009, 111(5), 2597-2606.
- 30 M. Born and E. Wolf, Principles of Optics: Electromagnetic Theory of Propagation, Interference and Diffraction of Light, Elsevier, 2013.

- 31 K. J. Pascoe, Reflectivity and Transmissivity through Layered, Lossy Media: A User-Friendly Approach. AIR FORCE INST OF TECH WRIGHT-PATTERSONAFB OH SCHOOL OF ENGINEERING, 2001.
- 32 F. Schenk, B. D. Wilts and D. G. Stavenga, The Japanese jewel beetle: a painter's challenge, Bioinspiration Biomimetics, 2013, 8(4), 045002.
- 33 M. Skoge, A. Donev, F. H. Stillinger and S. Torquato, Packing hyperspheres in high-dimensional Euclidean spaces, Phys. Rev. E, 2006, 74(4), 041127.
- 34 M. Anderson, R. Motta, S. Chandrasekar and M. Stokes, Proposal for a Standard Default Color Space for the InternetsRGB. In: Color Imaging Conference. vol. 6; 1996.
- 35 B. R. Sveinbjörnsson, R. A. Weitekamp, G. M. Miyake, Y. Xia, H. A. Atwater and R. H. Grubbs, Rapid self-assembly of brush block copolymers to photonic crystals, Proc. Natl. Acad. Sci. U. S. A., 2012, 109(36), 14332-14336.